Cell, Vol. 98, 537–546, August 20, 1999, Copyright ©1999 by Cell Press

Structure of the α-Actinin Rod: Molecular Basis for Cross-Linking of Actin Filaments

Kristina Djinović-Carugo, Paul Young, Mathias Gautel, and Matti Saraste*
Structural Biology Programme
European Molecular Biology Laboratory
Postfach 10.2209
D-69012 Heidelberg
Germany

Summary

We have determined the crystal structure of the two central repeats in the α-actinin rod at 2.5 Å resolution. The repeats are connected by a helical linker and form a symmetric, antiparallel dimer in which the repeats are aligned rather than staggered. Using this structure, which reveals the structural principle that governs the architecture of α-actinin, we have devised a plausible model of the entire α-actinin rod. The electrostatic properties explain how the two α-actinin subunits assemble in an antiparallel fashion, placing the actin-binding sites at both ends of the rod. This molecular architecture results in a protein that is able to form cross-links between actin filaments.

Introduction

α-Actinin is a ubiquitously expressed protein that is regarded as the ancestral molecule within a family of actin-binding proteins that includes spectrin, dystrophin, and utrophin (Blanchard et al., 1989; Pascual et al., 1997a). Muscle and nonmuscle isoforms of α-actinin have been characterized (Blanchard et al., 1989). In general, the nonmuscle isoforms bind to F-actin in a calcium-sensitive manner, whereas actin binding of the muscle isoforms is not controlled by calcium. In skeletal and cardiac muscle, α-actinin is found in the Z disk, where it cross-links antiparallel actin filaments from adjacent sarcomeres (Figure 1A). Interactions between α-actinin and titin may play a role in controlling Z disk assembly (Ohtsuka et al., 1997; Young et al., 1998). In nonmuscle cells, α-actinin is involved in the organization of the cortical cytoskeleton adjacent to membrane-associated structures such as zonula adherens and tight junctions. In cultured fibroblasts, it is localized at focal contacts or along stress fibers (see Blanchard et al., 1989 and references therein). In these structures, α-actinin not only cross-links actin filaments but also interacts with numerous cytoskeletal and membrane-associated proteins. It may link the actin cytoskeleton to the membrane either directly, via interactions with transmembrane receptors such as integrins, ICAMs, L-selectin, and the NMDA receptor (Otey et al., 1990; Carpen et al., 1992; Pavalko et al., 1995; Heiska et al., 1996; Wyszynski et al., 1997), or indirectly, via cytoskeletal proteins such as vinculin (Wachsstock et al., 1987; Figure 1B).

*To whom correspondence should be addressed (e-mail: saraste@embl-heidelberg.de).

α-Actinin is composed of an amino-terminal actin-binding region consisting of two calponin homology (CH) domains, a central rod containing four spectrin-like repeats, and a calmodulin-like domain at the carboxy terminus (Castresana and Saraste, 1995; Trave et al., 1995; Davison and Critchley, 1988). It is a dimer composed of two 100 kDa monomers that are arranged in an antiparallel manner to form a rod-shaped molecule with an actin-binding region at either end (Figure 1C). This arrangement allows α-actinin to cross-link actin filaments into tight bundles. Other proteins of the family (spectrin and dystropin) are composed of the same building blocks but differ in the number of repeats that separate the actin-binding regions in the oligomeric structures. The length of the spacer determines the final structure of the higher-order cytoskeletal assembly in the cell.

The repeats are characteristic of the entire family and contain from 100 to 120 residues. They were identified as homologous repeats in the sequence of α-spectrin (Speicher and Marchesi, 1984) and were later discovered in α-actinin and dystrophin (Davison and Critchley, 1988). The repeats are independent folding units, as shown by structural studies on a single repeat (Pascual et al., 1997b) and by unfolding studies using atomic force microscopy on spectrin and α-actinin repeats (Rief et al., 1999).

The crystal structure of the 14th repeat from the *Drosophila melanogaster* α-spectrin (Yan et al., 1993) and solution structure of the 16th repeat from the chicken brain α-spectrin (Pascual et al., 1997b) show that the repeat is an antiparallel triple-helical structure. The helices within the repeats show the heptad sequence pattern, which is commonly found in extended α-helical structures (McLachlan and Stewart, 1975). When the positions are canonically labeled from *a* to *g*, the residues *a* and *d* are generally hydrophobic and located on the inward-facing surface of the helix. These residues form the core of the domain and stabilize its fold by hydrophobic interactions. They are well conserved in the sequence alignments of homologous repeats in spectrins and α-actinins (Pascual et al., 1997a). Yan et al. (1993) have proposed a model in which successive repeats are connected by a long continuous α helix. The structure of two consecutive repeats from the chicken α-spectrin confirms the presence of a long helical connection between the repeats that may form a structural basis for the flexibility of the spectrin molecule (Grum et al., 1999 [this issue of *Cell*]).

Dimerization of α-actinin and spectrin is thought to be largely due to the contacts between the subunits that are mediated by the repeats (Imamura et al., 1988; Kahana and Gratzer, 1991; Speicher et al., 1992; Viel and Branton, 1994). In spectrin, a nucleation site for the formation of the α/β heterodimer has been found near one end of the molecule, and dimerization is proposed to proceed in a zipper-like fashion (Speicher et al., 1992). The arrangement of the spectrin-like repeats in the α-actinin homodimer (hereafter referred to as R1 to R4) is often depicted in an aligned assembly (Figure 1C$_l$). However, a staggered model has been proposed based

on projection images from two-dimensional crystals of α-actinin. In this model, either R1 or R4 does not pair with any repeat of the opposing monomer (Figures $1C_{II}$ and $1C_{III}$; Taylor and Taylor, 1993). Studies on the dimerization of expressed fragments containing either three or four repeats strongly support the aligned arrangement (Flood et al., 1995, 1997), whereas chemical cross-linking has not distinguished between the aligned and staggered models (Imamura et al., 1988).

Here we present the structure of the two central repeats (R2R3) of the muscle α-actinin, as determined by X-ray crystallography at 2.5 Å resolution. The crystal structure shows that the two-repeat segments form a symmetric, antiparallel dimer and reveals the structural principle that governs the architecture of the entire α-actinin rod and gives the protein the ability to form cross-links between actin filaments.

Results and Discussion

Structure Determination

The central repeats R2R3, corresponding to residues 371–637 of the human skeletal muscle α-actinin 2, crystallized in space group $P6_522$ with one molecule per asymmetric unit. Experimental phases were determined using multiwavelength anomalous dispersion (MAD) of the mercury derivative (Table 1). The solvent-flattened electron density map was readily interpretable and allowed positioning of most of the backbone of R2R3 and about 65% of the side chains. This model was submitted to several cycles of refinement and model building. The final refined model has a free R value of 31.0%, a conventional crystallographic R value of 22.8% (using all data to 2.5 Å), and consists of 248 amino acid residues and 123 water molecules. The number of water molecules is in agreement with the statistical analysis on experimentally located solvent molecules in protein crystal structures (Carugo and Bordo, 1999).

Structure of the Double Repeat

The three-dimensional structure consists of two repeats connected by a helical linker (Figure 2A). The molecule has an elongated shape with a length of 130 Å and a diameter of about 20 Å. The fold of each repeating unit is determined by three α helices in a coiled-coil assembly. In the following, we shall refer to the helices of the first repeat as 1, 2, and 3 and the helices of the second repeat as 1′, 2′, and 3′.

The two repeats are structurally very similar. The superposition of R2 and R3 results in a 1.36 Å rms distance of 84 equivalent Cα atoms (Figure 2B), and the rms distances between the Cα atoms of repeat R16 of α-spectrin (Pascual et al., 1997b) and R2 and R3 are 1.37 Å and 1.40 Å (on 64 Cα atoms), respectively. The major structural difference between R2 and R3 resides in the loop connecting the second and the third helix (loop 2-3/2′-3′). In R2, helices 2 and 3 are connected by a β turn, whereas the corresponding region in R3 is much longer, with residues 209–215 protruding toward the helix 1′ (for residue numbering, see Figure 6A). The loop conformation is locked in this position by several interactions with helix 1. The second prominent difference is found in the C-terminal part of the last helix. In

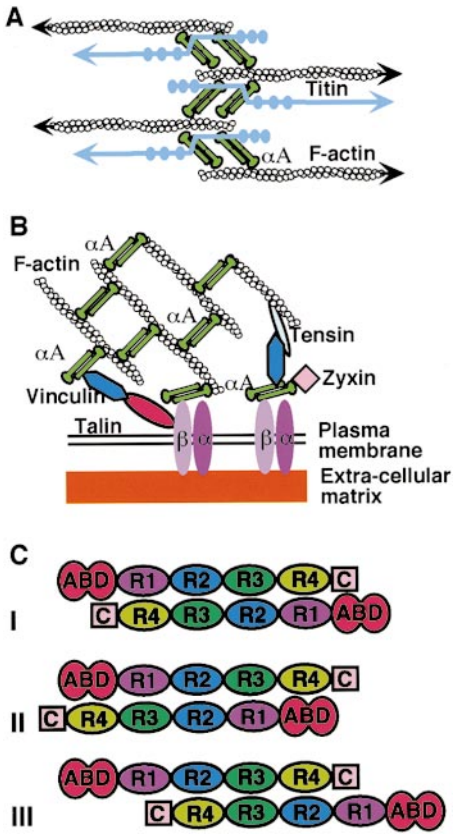

Figure 1. Domain Structure of α-Actinin and Its Function in the Sarcomeric Z Disk and in Focal Contacts

(A) In the muscle Z disk, α-actinin (αA) cross-links antiparallel actin filaments from adjacent sarcomeres. Titin acts as a molecular ruler for the sarcomere and interacts with two different parts of α-actinin, at the center of the α-actinin rod and with the calmodulin-like domain (Gregorio et al., 1999). These interactions may play a role in controlling the thickness of the Z disk (Young et al., 1998).

(B) A simplified representation of a focal contact showing α-actinin linking the actin cytoskeleton to membrane-associated structures. Focal contacts are points where cultured cells are attached tightly to the extracellular matrix via transmembrane receptors such as integrins (α and β in figure) (Burridge and Chrzanowska-Wodnicka, 1996). α-Actinin has been shown to interact with β integrins (Otey et al., 1990) as well as with the focal contact components vinculin (Wachsstock et al., 1987) and zyxin (Crawford et al., 1992). Thus, it may connect integrins to actin filaments either directly or indirectly, involving proteins such as talin (Horwitz et al., 1986) or tensin (Beckerle, 1997).

(C) Domain structure of α-actinin showing aligned and staggered models for the dimer. ABD, actin-binding domain; R1, R2, R3, and R4, repeats; C, C-terminal calmodulin-like domain. The color scheme for the repeats is maintained throughout the paper. (I), an aligned arrangement where R1 and R2 are paired with R4 and R3, respectively, of the opposing monomer; (II) and (III), alternative staggered arrangements where either R1 or R4 is not paired with any repeat of the opposing monomer.

R2, helix 3, which connects to R3 through the helical linker, has a linear conformation stabilized by interactions with R3. The end of helix 3′ in R3 is bent toward the core of the protein, but its conformation may be more linear when the R4 repeat is present (see below).

Apart from the hydrophobic packing in the core, electrostatic interactions also contribute to the stabilization

Table 1. Data Collection and Refinement Statistics

	λ1	λ2	λ3	Native
Data Collection				
Wavelength (Å)	0.8265	1.0078	0.9183	0.947
Space group		$P6_522$		
Cell (Å)		a = b = 60.59 c = 390.47		a = b = 60.05 c = 390.81
Unique reflections	10,194	10,194	10,072	21,275
Resolution (Å)	2.9	2.9	2.9	2.2
Redundancy	6.4	7.4	6.4	6.1
Completeness (%)	97.8(96.7)[a]	97.5(98.0)	97.4(99.4)	94.6(89.8)
R_{merge}[b]	0.069(0.136)	0.050(0.155)	0.052(0.135)	0.062(0.339)
Phasing				
Figure of merit (55.0–2.9 Å)[c] (centric/acentric)	0.510/0.375	0.537/0.391	0.530/0.394	
Refinement				
No. of reflections				14,585
Resolution				2.5
R factor[d]				0.228
R_{free}[e]				0.310
Nonhydrogen atoms				2,158
Protein atoms				2,035
Water molecules				123
Bond lengths (Å)				0.0097
Bond angles (°)				1.27
Overall B value (Å^2)				57.2

[a] Numbers in parentheses refer to the last resolution shell.
[b] $R_{merge} = \Sigma|I_i - \langle I\rangle|/\Sigma I_i$, where I_i is the intensity of an individual reflection and $\langle I\rangle$ is the mean intensity of that reflection.
[c] Figure of merit = $\langle|\Sigma P(\alpha)e^{i\alpha}/\Sigma P(\alpha)|\rangle$, where α is the phase and P(α) is the phase probability distribution.
[d] R factor = $\Sigma\ |F_o - F_c|/\Sigma F_o$.
[e] R_{free} is the cross-validation R factor computed for the test set of reflections (8% of the total) that are omitted in the refinement process.

of the repeat fold. Salt bridges and hydrogen bonds between oppositely charged residues can be grouped into two classes: intrahelical interactions between residues spaced at i, i + 3, or i + 4 intervals, and interhelical contacts that contribute to the tertiary structure of each repeat. Both types of interactions can be observed in α-helical structures (Lyu et al., 1992; Kohn et al., 1998) and are known to stabilize α helices and coiled-coil assemblies. The residues involved in these interactions are not strictly conserved either in R2 or R3 nor generally in the α-actinin repeats. However, functionally analogous contacts are observed when R2 and R3 structures

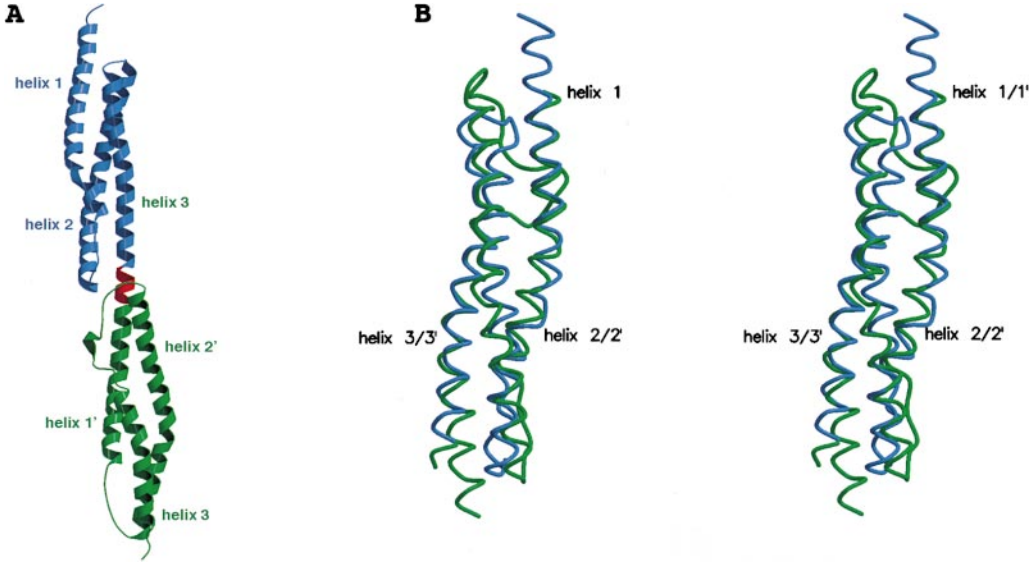

Figure 2. Overall Structure of R2R3 and Structural Comparison of the Repeats

(A) R2 is colored blue, R3 is green, and the linker segment is red. All ribbon diagrams were generated using the programs MOLSCRIPT (Kraulis, 1991) and Raster3D (Merritt and Murphy, 1994).

(B) Stereoview of the superposition of the helices in R2 and R3. Coloring is as depicted above.

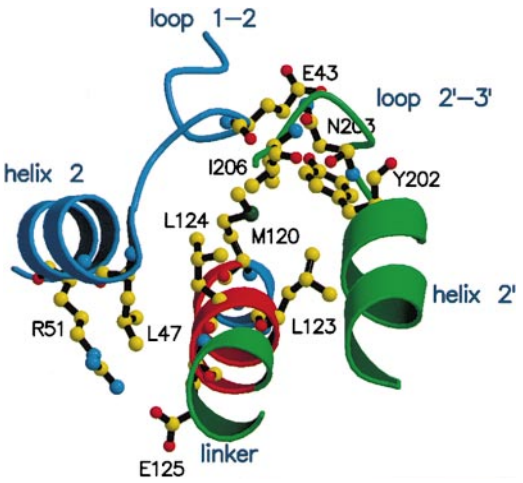

Figure 3. The Connecting Linker

Close-up of interactions between R2, R3, and the linker. The protein backbone is shown as a ribbon, and amino acid residues are drawn in a ball-and-stick representation. R2 is colored blue, R3 is green, and the linker is red.

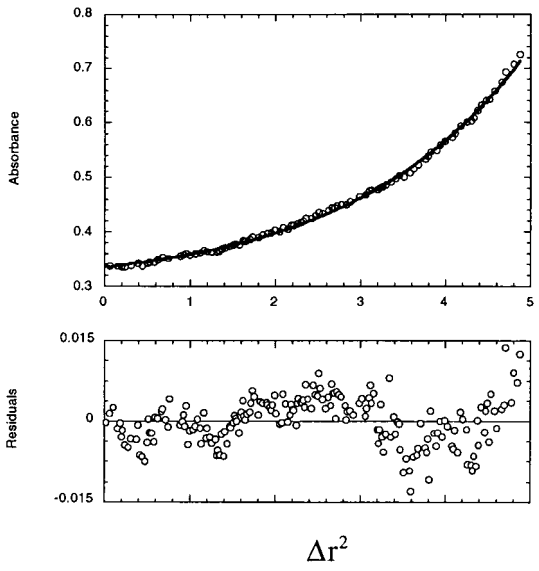

Figure 4. Sedimentation Equilibrium

Analytical ultracentrifugation was carried out as described in the Experimental Procedures. The figure shows absorbance at 293 nm versus Δr^2, where r is the radial position. The experimental data is shown as open circles and the fitted data as a continuous line. The bottom shows the residuals (open circles) expressed as the difference between the experimental and the fitted data.

are compared. Interestingly, only one such ion pair involves residues coming from the two consecutive repeats (Arg51–Glu125) and joins helix 2 of R2 to the linker, connecting the two repeats (Figure 3).

Helical Linker

The boundaries of repeats in α-actinin have been extensively studied by limited proteolysis. According to our structure, the N-terminal boundaries of proteolytically stable constructs, as defined by Gilmore et al. (1994) for R3 and R4, are located within the third helix of the preceding repeat. This may indicate that the C-terminal helix of the repeat, the N-terminal helix of the following repeat, and the helical linker form a stable, folded structural moiety.

The linker region between the two repeats can be determined by an analysis of the gradient of atomic displacement parameters. A sharp and sudden increase of the gradient of atomic displacement parameters is observed between residues Met-120 and Glu-125 at the three-dimensional interface of the two repeats that meet along the connecting helix at residue 122. The segment 120–126 is flanked by the structural elements of the two consecutive repeats, in particular by loop 1-2 and helix 2 and loop 2′-3′ and helix 2′. One side of the linker helix is exposed to the solvent (Figure 3).

We define the α-helical section, which is colored red in Figures 2A and 3, as the linker between the two consecutive repeats. The interactions within the linker region are centered at the hydrophobic residues Leu-123 and Leu-124, which make van der Waals contacts both to the residues of R2 (Leu-47) and R3 (Ile-206 and Tyr-202; the latter also contacts the side chain of Met-120). Apart from this hydrophobic cluster, additional polar interactions between the residue pairs Glu43–Asn203 (a side chain–to–side chain hydrogen bond) and Arg51–Glu125 (a salt bridge) stabilize the repeat interface. These residues are highly conserved in α-actinins (Blanchard et al., 1989), suggesting that this interaction geometry between repeats R2 and R3 is a structural feature of the family. An exception is α-actinin from *Dictyostelium discoideum*, in which the 2′-3′ loop is seven residues shorter and must adopt a different local conformation.

The relative orientation of the two repeats is described by a translation of about 55 Å along the connecting helix and a rotation by approximately 100 degrees around the same axis. A proline residue at position 140 induces a bend of 21 degrees in the connecting helix. The presence of a proline at this position is a conserved feature within the α-actinin family, but proline is not preserved in all repeats within the α-actinin molecule. Thus, the connecting helices between other repeats could adopt variable conformations in this region and have different degrees of bending.

The Antiparallel Dimer

We have analyzed the oligomeric state of the R2R3 construct with several techniques and at various concentrations. Yeast two-hybrid analysis, size-exclusion chromatography, and analytical ultracentrifugation clearly indicate that the R2R3 construct forms a stable dimer in solution at concentrations between 1–50 mg/ml. The analytical centrifugation data (Figure 4) show that the sample is a homogeneous dimer with a molecular weight of 60.8 kDa, in good agreement with the theoretical value of 58.5 kDa. K_d for the monomer/dimer dissociation can be estimated to be 2 μM. The crystal structure also shows a dimer formed by a crystallographic 2-fold axis, which is perpendicular to the long molecular axis and centered at the middle of the dimer. The dimer is assembled in an aligned, antiparallel manner (Figure 5A). The two monomers are in contact along the whole length of

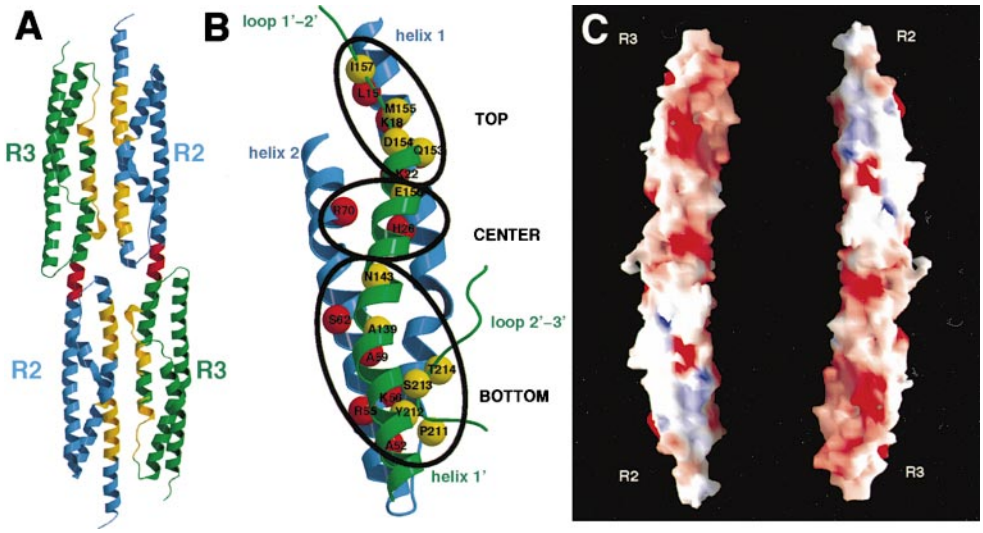

Figure 5. Structure of the R2R3 Dimer and the Interface

(A) Ribbon diagram of the antiparallel R2R3 dimer. R2 is blue, R3 is green, the linker is red, and the structural elements involved in the dimer interface are yellow.

(B) Dimer interface. The protein backbone is shown as a ribbon, and the residues involved in the dimer interface are depicted as red balls for R2 and yellow balls for the opposing R3, centered on the Cα atom of the residues.

(C) Electrostatic surface potential of the R2R3 dimer interface. Surfaces are colored by electrostatic potential. Positive regions are depicted in blue and negative in red. The second subunit (right) was rotated by 180 degrees to show charge complementarity in the dimer interface. Figure was generated with GRASP (Nicholls et al., 1991).

the molecule, and 9.2% (1460 Å^2) of the monomer surface is buried upon dimer formation. This value is in good agreement with corresponding values for stable homodimers (Jones and Thornton, 1996).

In the dimer interface, helix 1′ and loop 1′-2′ of R3 face the groove formed by helices 1 and 2 of R2 in the opposing monomer (Figure 5B). The C-terminal region of helix 1′ and the subsequent loop 1′-2′ of R3 interact with the N-terminal part of helix 1 in R2 (top). The central part of the helix 1′ interacts with both helices 1 and 2 (center), whereas the N-terminal part of helix 1′, together with the protruding loop 2′-3′, contacts only helix 2 of R2 (bottom). These interactions, which are lined along the longitudinal direction of the R2R3 structure, are repeated in the second half of the dimer due to the 2-fold symmetry axis perpendicular to the long molecular axis. In total, 38 residues per monomer can be considered to be at the dimer interface, as judged by the decrease in solvent-accessible area upon dimer formation.

The contacts at the top of the dimer consist of a hydrophobic cluster and specific polar interactions. Loop 1′-2′ (R3) is lined above helix 1 (R2) and stabilized in this position by hydrophobic interactions to the underlying N-terminal part of helix 1. Additionally, a salt bridge and a main chain–to–main chain hydrogen bond are involved in contacts between residues from loop 1′-2′ and helix 1 (Figure 5B). In the center, the interface is formed by two solvent molecules that establish a hydrogen bonding network connecting Glu-150 (helix 1′) to His-26 (helix 1) and His-67 (helix 2) and to the carbonyl oxygen of Lys-22 (helix 1). These interactions join two α helices in R2 and one helix in R3 of the other subunit. Additionally, a salt bridge between Arg-70 (helix 2) and Glu-150 (helix 1′) contributes to the stability of the α-actinin dimer in this region.

At the bottom end of the R2–R3 interface, helices 2 and 1′ interact through a hydrogen bonding network bridged by a solvent molecule and through van der Waals interactions between two small hydrophobic residues. The interactions between the two monomers continue through contacts between the helix 2 residues and the protruding part of the loop 2′-3′, involving residues 211–214. Several direct polar interactions, as well as solvent-mediated hydrogen bonds involving side chain and main chain atoms, are found in this region. Moreover, a small hydrophobic cluster centered around Tyr-212 (loop 2′-3′) is formed upon dimerization. Finally, a hydrogen bond between the two symmetry-related Thr-48 residues in the opposing subunits terminates the dimer interface at the proximity of the 2-fold axis.

The majority of interactions in the dimer interface are polar, and some of them are modulated by solvent molecules that assist the continuation of the hydrogen bonding network connecting the subunits. The predominantly polar character of the contacts between the two subunits is likely to be the basis of salt-induced conformational changes of α-actinin observed by electron microscopy and viscosity measurements (Kuroda et al., 1994; Winkler et al., 1997).

Analysis of the electrostatic surface potential of the dimer interface (Figure 5C) shows complementarity between the interacting surfaces in terms of productive electrostatic interactions between the two monomers. In a staggered model (Figures 1C$_{II}$ and 1C$_{III}$), the juxtaposition of R2 or R3 would result in a number of repulsive interactions between equally charged residues and prevent the dimerization.

The structural elements involved in the interface lead to the formation of a perfectly aligned, antiparallel homodimer (Figure 1C$_{I}$). Most of the residues in the interface

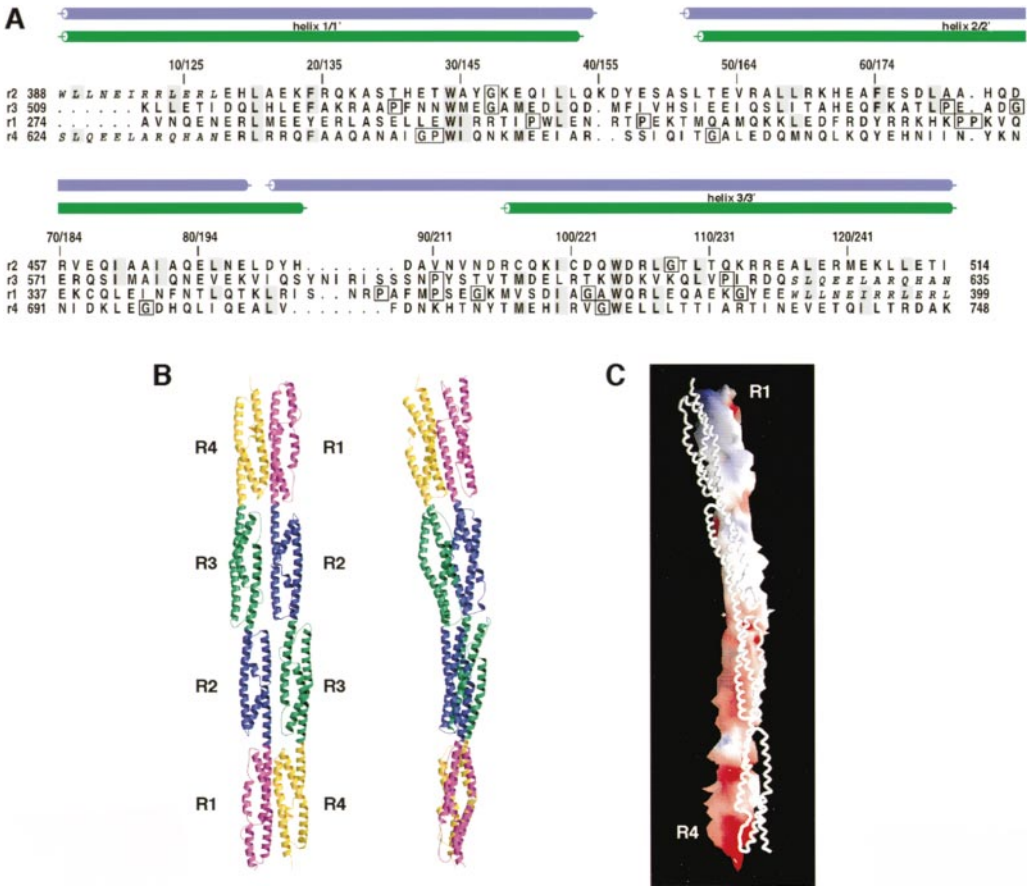

Figure 6. Model of the α-Actinin Rod

(A) Sequence alignment of the α-actinin repeats used in modeling of repeats R1 and R4. Residue numbers for the full-length molecule and those of the construct used for the crystal structure are indicated at the edges and above the alignment, respectively. The α helices seen in the crystal structure are depicted as bars (blue for R2 and green for R3). The C termini of R1 and R3 and the N termini of R2 and R4, respectively, overlap due to the modeling procedure of R1 and R4. The overlapping residues shown in italic were used to assemble the model of the rod. The figure was generated with ALSCRIPT (Barton, 1993).

(B) Ribbon diagram of α-actinin rod viewed in two orientations related by a 65 degree rotation around the long molecular axis through the central 2-fold axis. R1 is colored violet, R2 is blue, R3 is green, and R4 is yellow.

(C) Electrostatic surface potential of one R1–R4 subunit generated with GRASP (Nicholls et al., 1991). Positively charged surface is colored blue and negatively charged red. The second subunit is white in a wormlike representation. Surfaces corresponding to R1 and R4 are marked.

are well conserved within the α-actinin sequences (Blanchard et al., 1989). This is expected, as disruptive mutations affecting residues involved in the dimer interface would have a double effect on its stability due to the 2-fold symmetry.

α-Actinin Rod

In order to further elucidate the molecular basis for cross-linking of actin filaments by α-actinin, we have constructed a model of the α-actinin rod, comprising repeats R1–R4. A homology model of the monomeric rod was built using the three-dimensional structures of domains R2 and R3 as templates for modeling repeats R4 and R1, respectively, as described under Experimental Procedures, using the sequence alignment shown in Figure 6A. The antiparallel dimer (Figure 6B) was constructed by application of the crystallographic 2-fold axis, which relates the two monomers in the crystal structure of R2R3. The relative orientation of repeats R1 and R2 in the monomeric rod can be described by a rotation of about 120 degrees around the connecting helix, together with a translation of approximately 55 Å along the same axis. Similar rotations and translations (125 degrees and 60 Å) characterize spatial relations between repeats R3 and R4. The model of the monomeric rod deviates by 20 degrees from linearity.

The dimer is around 240 Å long and 40 Å wide and displays a twist of 73 degrees. These dimensions are in a good agreement with electron microscopic data on the intact α-actinin (22.5 ± 2.1 nm; Flood et al., 1995) and on the polypeptide released from α-actinin by thermolytic digestion (22.5 nm × 5.9 nm; Winkler et al., 1997). 3380 Å^2 (12%) of the solvent-accessible area in the monomer is involved in the dimer interface, which continues throughout the long molecular axis and involves all four repeats. The organization of the α-actinin rod brings helix 3 of R4 and helix 3 of the opposing R1 into proximity. The interactions between these two moieties are based on polar contacts. Additional polar interactions between repeats R1 and R4 involve the two pairs

of structural elements: helix 3 of R4 and helix 2 of R1, and loop 2-3 of R4 and helix 3 of R1.

A number of experiments employing different methods have been used to address the question of the intersubunit interactions within the α-actinin homodimer. EM studies on chicken gizzard α-actinin in negative stain (Taylor and Taylor, 1993) and under different salt conditions (Winkler et al., 1997) support staggered models (Figures $1C_{II}$ and $1C_{III}$) and suggest conformational changes induced by a variation of ionic strength. Also, EM experiments on fragments containing repeats 1–4, 1–3, and 2–4 can be interpreted as being consistent with a staggered model (Flood et al., 1995). However, none of these EM studies are at sufficiently high resolution to allow unambiguous identification of the individual repeats, and as pointed out by Flood et al. (1995), it is not clear whether the α-actinin dimer retains its native structure under the harsh conditions used for sample preparation in some EM experiments.

Biochemical data based on cross-linking and analysis of association by sedimentation equilibrium of different constructs containing repeats R1–R4, R2–R4, and R1–R3 have shown that in order to generate a maximally stable antiparallel dimer, all four repeats are required. This suggests that they all contribute to the dimer interface and indicates their aligned pairing. In addition, our yeast two-hybrid experiments on double repeat constructs indicate that R1R2 interacts with R3R4 and that R2R3 interacts with itself, consistent with an aligned model. No interactions are observed between R2R3 and either R1R2 or R3R4, arguing against a stagger within the rod in either direction (Figure 1C; P. Y., unpublished results).

In our model, the repeats of opposing subunits in the dimer (Figure 6B) interact in a pairwise manner corresponding to the aligned model. The model is in good agreement with the biochemical studies mentioned above. The isolated rod dimer is extremely stable (Imamura et al., 1988; Kahana and Gratzer, 1991; Flood et al., 1995), suggesting that the N- and C-terminal domains of α-actinin do not make a dominant contribution to dimerization. Thus, we expect that the arrangements of the repeats in our model closely resemble that of the full-length molecule. Given the high sequence conservation in the α-actinin rod between the muscle and nonmuscle isoforms (Beggs et al., 1992), it is almost certain that the aligned model holds true for both.

The electrostatic potential of the monomeric rod (Figure 6C) shows a pronounced polarity of the molecule, with a positive charge at the N terminus and a negative charge at the C terminus. In the aligned, antiparallel assembly of subunits, oppositely charged repeats are brought in optimal juxtaposition, stabilizing the dimer interface. Inspection of the level of amino acid identity between the α-actinin repeats (Figure 6A) shows that R1 and R4 have diverged further during their evolution with respect to R2 and R3. This is expected, since their prominent charge complementarity is required for the optimal fit between subunits. Taken together, the analysis of the dimer interface along with biochemical data strongly supports the aligned, antiparallel model for the α-actinin dimer.

Biological Implications

α-Actinin links diverse cellular structures to the actin cytoskeleton in many different cell types. The binding sites of many ligands have been mapped to the α-actinin rod. In the Z disk of muscle, these partner proteins include titin and a LIM protein, which both appear to interact with the α-actinin rod (Xia et al., 1997; Young et al., 1998). The rod region also binds to the cytoplasmic tail of the NMDA receptor (Wyszynski et al., 1997). R3 of both skeletal and nonmuscle α-actinin may interact with the Rho-activated protein kinase PKN (Mukai et al., 1997). The interactions between α-actinin and the cytoplasmic domains of the transmembrane receptors β1 integrin and L-selectin have been mapped to the rod (Otey et al., 1990; Pavalko et al., 1995). Our structure may help to study these interactions in more detail.

Molecular architecture of the α-actinin dimer forms the basis of its primary function, cross-linking of actin filaments. The repeats of the rod define the elongated shape of the molecule as well as the antiparallel association of the subunits that places the functional domains (calmodulin-like domain and actin-binding region) at the ends of the molecule. In skeletal and cardiac muscle, α-actinin cross-links antiparallel actin filaments coming from adjacent sarcomeres (Figure 1). The symmetry axis at the center of the rod can easily lead to the antiparallel arrangement of actin-binding sites in the dimer, which is complementary to the antiparallel orientation of actin filaments in the Z disk. In nonmuscle and smooth muscle cells, actin filaments are not part of an ordered lattice peculiar to the Z disk and can assume variable orientations. In order to accomplish actin bundling under these conditions, the actin-binding domain must be able to change its orientation via a built-in flexibility in the neck connecting it to the rod. The fact that the actin-binding fragment can be isolated from the rod by limited proteolytic digestion (Imamura et al., 1988) indicates such an inherent flexibility of this neck. A principal feature that distinguishes the muscle and nonmuscle α-actinins is the ability of the latter to bind actin filaments in a calcium-sensitive manner (Landon et al., 1985). Calcium concentrations higher than 10^{-7} M abolish binding. The antiparallel orientation of the subunits makes it possible that the binding of calcium to the calmodulin-like domain of one subunit sterically prevents actin binding of the neighboring subunit via a conformational change. Elucidation of this mechanism will require the structure determination of the entire α-actinin molecule.

Experimental Procedures

Preparation and Crystallization of the R2R3 Construct

A DNA fragment corresponding to amino acids 371 to 637 of human skeletal muscle α-actinin 2 (ACTN2; EMBL database M86406) was amplified from a human cardiac cDNA library (Clontech) by polymerase chain reaction. This region contains the spectrin-like repeats 2 and 3 (R2R3) as determined by Gilmore et al. (1994) for chicken cytoskeletal α-actinin. This fragment was cloned into a pET 8c vector (Novagen) modified such that the R2R3 polypeptide contains the additional N-terminal amino acid sequence MHHHHHHSTEN LYFQGSS when expressed in *Escherichia coli* BL21[DE3]. Induction of expression was carried out at 37°C using 0.2 mM IPTG. Absence of mutations was verified by DNA sequencing. Initial purification was carried out on an Ni-NTA agarose column (Qiagen) followed by removal of the N-terminal tag using TEV protease (GIBCO-BRL)

(Parks et al., 1994). This results in an α-actinin R2R3 polypeptide containing three additional N-terminal residues, GSS. This untagged polypeptide was collected in the flowthrough fraction of a second Ni-NTA column and further purified by ion exchange on a MonoQ column (Pharmacia). The protein was then dialyzed to 20 mM Tris-HCl (pH 7.4), 1 mM DTT and concentrated to 150 mg/ml for crystallization. Crystals were grown using vapor diffusion at 4°C or 17°C by mixing the protein in a 1:1 volume ratio with a solution containing 26% PEG 400 (Fluka), 100 mM $MgSO_4$, and 100 mM HEPES or Tris-HCl (pH 7.5–8.0). Crystals were hexagonal bipyrimids and had dimensions of up to 0.5 mm. The high protein concentration is necessary to obtain crystals under these conditions.

Data Collection and Structure Determination

Crystals were harvested in a stabilization buffer containing 30% PEG 400, 100 mM $MgSO_4$, and 100 mM HEPES and frozen in a liquid nitrogen–cooled stream. All data were integrated and reduced with the DENZO/SCALEPACK programs (Otwinowski and Minor, 1997), whereas subsequent manipulations of diffraction data were performed using the CCP4 suite of programs (CCP4, 1994). Crystals formed in space group $P6_522$, with unit cell dimensions of $a = b = 60.05$ Å, $c = 390.81$ Å, and contain one R2R3 molecule in the asymmetric unit with a solvent content of approximately 65%. All data were collected at the European Synchrotron Radiation Facility (ESRF) in Grenoble, France. A native data set to 2.2 Å resolution was collected at ID14-3 beamline on an off-line image plate with dimensions 400 mm × 800 mm using a wavelength of 0.947 Å (Table 1). Derivatives were identified from diffraction data collected at beamline BM2 on a CCD detector. A mercury derivative was prepared by soaking the crystals in the stabilization buffer with 1 mM thiomersal for 12 hr.

MAD data were collected to 2.9 Å resolution from mercury-derivatized crystal at three wavelengths: at the dip of the LIII absorption edge of mercury, and at two energies above the LI and LIII edges, respectively, using beamline BM14 and Mar345 image plate detector (Table 1). A fluorescence scan on derivatized crystal was taken to optimize data collection parameters. The scaled and reduced intensity data were converted to amplitudes using TRUNCATE, and cross-wavelength scaling was performed using SCALEIT of CCP4. Two mercury sites were identified in the anomalous and dispersive Patterson maps, using the program RSPS (CCP4). These sites were further refined with the program PHASES (Furey and Swaminathan, 1997). Additionally, the native data set was included in the phasing process. The handedness of the heavy atom sites was determined by inspecting 3.0 Å resolution MIRAS maps calculated with the mercury sites in both possible hands and both enantiomorphic space groups. Clear electron density for several helices in the R2R3 construct defined the hand of the heavy atom sites unambiguously. Mercury sites were subsequently refined by SHARP (de la Fortelle and Bricogne, 1997), resulting in a final overall figure of merit of 0.72 (30.0 to 2.9 Å). The phases were further improved with solvent flipping using the program SOLOMON (CCP4), resulting in an electron density map to which most of the backbone and about 65% of the side chains were readily positioned using O (Jones et al., 1991). Due to anisotropic diffraction along the direction perpendicular to b^*, the data to 2.5 Å resolution were used during refinement.

Refinement of the model by CNS (Brünger et al., 1998) utilized the native data set (Table 1) with the maximum likelihood target function (Pannu and Read, 1996). Corrections for the bulk solvent were applied during the refinement. Weighting schemes (Read, 1986), as implemented in CNS, were used throughout for map calculations. Several cycles of model building and refinement were performed to produce the final refined model at 2.5 Å resolution, with a crystallographic R value of 22.8% and a free R value of 30.2%. This model consists of residues 371–635 of the human skeletal muscle α-actinin 2 and 123 water molecules. PROCHECK (Laskowski et al., 1993) was used to gauge the stereochemical quality of the final model. The Ramachandran plot has 89.7% of the residues lying in the most favored and 9.5% in the allowed regions. The two residues in unfavorable regions have weak density and are located at the extended N terminus of the construct (GSS). Refined overall temperature factors of 57.2 $Å^2$ (54.9 $Å^2$ for main chain atoms, 59.2 $Å^2$ for side chain atoms, and 58.9 $Å^2$ for water molecules) are consistent with the 48.6 $Å^2$ overall thermal factor obtained from Wilson scaling of the diffraction data (CCP4).

Analytical Ultracentrifugation

Sedimentation equilibrium studies of R2R3 were carried out on a Beckman Optima XL-A analytical ultracentrifuge using an An50Ti rotor at a protein concentration of 1 mg/ml in a buffer containing 20 mM Tris-Cl (pH 7.6) and 1 mM DTT. Centrifugation was carried out at 4°C and 11,000 rpm for 24 hr. Absorbance was monitored at 293 nm. The data were analyzed using the Ultrascan Version 2.98 package (B. Demeler, The University of Texas Health Science Center at San Antonio).

Construction of Homology Models of R1 and R4 and α-Actinin Rod

Sequence alignments were produced with CLUSTAL W-1.6 (Higgins et al., 1991) and edited with the SEQLAB program of the GCG package (Wisconsin Package Version 9.1, Genetics Computer Group [GCG], Madison, WI). The homology modeling of R1 and R4 repeats was carried out by first obtaining a reliable sequence alignment of repeats 1–4 of human skeletal muscle α-actinin 2 (Figure 6A). The R2 and R3 sequences were aligned based on the superposition of the Cα coordinates using program SUPERIMPOSE (Diederichs, 1995) to provide the best overall structural comparison. After this, a profile alignment with CLUSTAL W was performed between two groups of aligned amino acid sequences: (1) R2 and R3, and (2) multiple sequence alignment of spectrin, utrophin, and dystrophin repeats (Winder et al., 1995). Alignment 1 contained secondary structure assignments for gap penalty mask. This step produced the final profile against which R1 and R4 sequences were aligned (Figure 6A). As R1 and R3 repeats both have an insertion between helices 2 and 3, R3 structure was used as the template for R1 modeling, whereas R2 was employed in modeling of repeat R4. Modeling was performed with the program suite MODELLER (Sali and Blundell, 1993). The monomeric rod of α-actinin was assembled by structural superposition of overlapping N-terminal and C-terminal regions (12 amino acid residues) of the R1 model and R2, and R3 and the R4 model (shown in italics in Figure 6A). This model was subjected to energy minimization using the X-PLOR program (Brünger, 1992) in order to release steric strain introduced during the model-building process. Antiparallel dimer was produced by application of symmetry operator $1 - X + Y, Y, -Z + 1/2$ on the monomer and submitted to energy minimization by X-PLOR. The model of α-actinin rod has a root-mean-square deviation of 0.012 Å from ideal bond lengths and 2.2° from ideal bond angles.

Acknowledgments

The authors wish to thank W. Burmeister, S. Wakatsuki, M. Roth, and A. Thompson at the ESRF synchrotron facility in Grenoble for excellent assistance with diffraction experiments. We are grateful to M. Way for critical reading of the manuscript; O. Carugo for helpful discussions about structure analysis; H. van der Zandt for help with analytical centrifugation experiments; and T. Gibson for constructive discussions on sequence alignments. We are grateful to R. MacDonald and A. Mondragón for communicating results prior to publication. This work was supported by the Deutsche Forschungsgemeinschaft grants Ga405/4-1 and Ga405/3-6.

Received June 16, 1999; revised July 13, 1999.

References

Barton, G.J. (1993). ALSCRIPT: a tool to format multiple sequence alignments. Prot. Eng. *6*, 37–40.

Beckerle, M.C. (1997). Zyxin: zinc fingers at sites of cell adhesion. Bioessays *19*, 949–957.

Beggs, A.H., Byers, T.J., Knoll, J.H., Boyce, F.M., Bruns, G.A., and Kunkel, L.M. (1992). Cloning and characterization of two human skeletal muscle α-actinin genes located on chromosomes 1 and 11. J. Biol. Chem. *267*, 9281–9288.

Blanchard, A., Ohanian, V., and Critchley, D. (1989). The structure and function of α-actinin. J. Muscle Res. Cell Motil. *10*, 280–289.

Brünger, A.T. (1992). X-PLOR, a System for Crystallography and NMR, Version 3.1, Manual Edition. (New Haven, CT: Yale University Press).

Brünger, A.T., Adams, P.D., Clore, G.M., DeLano, W.L., Gros, P., Grosse-Kunstleve, R.W., Jiang, J.-S., Kuszewski, J., Nilges, M., and Pannu, N.S., et al. (1998). Crystallography and NMR system (CNS): a new software suite for macromolecular structure determination. Acta Crystallogr. D *54*, 905–921.

Burridge, K., and Chrzanowska-Wodnicka, M. (1996). Focal adhesions, contractility, and signaling. Annu. Rev. Cell Dev. Biol. *12*, 463–518.

Carpen, O., Pallai, P., Staunton, D.E., and Springer, T.A. (1992). Association of intercellular adhesion molecule-1 (ICAM-1) with actin-containing cytoskeleton and α-actinin. J. Cell Biol. *118*, 1223–1234.

Carugo, O., and Bordo, D. (1999). How many water molecules can be detected by protein crystallography?. Acta Crystallogr. D *55*, 479–483.

Castresana, J., and Saraste, M. (1995). Does Vav bind to F-actin through a CH domain? FEBS Lett. *374*, 149–151.

CCP4 (Collaborative Computing Project No. 4). (1994). The CCP4 suite: programs for protein crystallography. Acta Crystallogr. D *50*, 760–763.

Crawford, A.W., Michelsen, J.W., and Beckerle, M.C. (1992). An interaction between zyxin and α-actinin. J. Cell Biol. *116*, 1381–1393.

Davison, M.D., and Critchley, D.R. (1988). α-Actinins and the DMD protein contain spectrin-like repeats. Cell *52*, 159–160.

de la Fortelle, E., and Bricogne, G. (1997). Maximum-likelihood heavy atom parameter refinement for multiple isomorphous replacement and multiwavelength anomalous diffraction methods. Methods Enzymol. *276*, 472–494.

Diederichs, K. (1995). Structural superposition of proteins with unknown alignment and detection of topological similarity using a six-dimensional search algorithm. Proteins *23*, 187–195.

Flood, G., Kahana, E., Gilmore, A.P., Rowe, A.J., Gratzer, W.B., and Critchley, D.R. (1995). Association of structural repeats in the α-actinin rod domain. J. Mol. Biol. *252*, 227–234.

Flood, G., Rowe, A.J., Critchley, D.R., and Gratzer, W.B. (1997). Further analysis of the role of spectrin repeat motifs in α-actinin dimer formation. Eur. Biophys. J. *25*, 431–435.

Furey, W.B., and Swaminathan, S. (1997). PHASES-95: a program package for the processing and analysis of diffraction data from macromolecules. In Methods in Enzymology, Vol. 277, C.W. Carter and R.M. Sweet, eds. (Orlando, FL: Academic Press), pp. 590–620.

Gilmore, A.P., Parr, T., Patel, B., Gratzer, W.B., and Critchley, D.R. (1994). Analysis of the phasing of four spectrin-like repeats in α-actinin. Eur. J. Biochem. *225*, 235–242.

Gregorio, C.C., Granzier, H., Sorimachi, H., and Labeit, S. (1999). Muscle assembly: a titanic achievement? Curr. Opin. Cell Biol. *11*, 18–25.

Grum, V.L., Li, D., MacDonald, R.I., and Mondragón, A. (1999). Structures of two repeats of spectrin suggest models for flexibility. Cell *98*, this issue, 523–535.

Heiska, L., Kantor, C., Parr, T., Critchley, D.R., Vilja, P., Gahmberg, C.G., and Carpen, O. (1996). Binding of the cytoplasmic domain of intercellular adhesion molecule-2 (ICAM-2) to α-actinin. J. Biol. Chem. *271*, 26214–26219.

Higgins, D.G., Bleasby, A.J., and Fuchs, R. (1992). CLUSTAL V: improved software for multiple sequence alignment. Comput. Appl. Biosci. *8*, 189–191.

Horwitz, A., Duggan, K., Buck, C., Beckerle, M.C., and Burridge, K. (1986). Interaction of plasma membrane fibronectin receptor with talin—a transmembrane linkage. Nature *320*, 531–533.

Imamura, M., Endo, T., Kuroda, M., Tanaka, T., and Masaki, T. (1988). Substructure and higher structure of chicken smooth muscle α-actinin molecule. J. Biol. Chem. *263*, 7800–7805.

Jones, S., and Thornton, J.M. (1996). Principles of protein-protein interactions. Proc. Natl. Acad. Sci. USA *93*, 13–20.

Jones, T.A., Zou, J.Y., Cowen, S.W., and Kjeldgaard, M. (1991). Improved methods for building protein models in electron density maps and the location of errors in these models. Acta Crystallogr. A *47*, 110–119.

Kahana, E., and Gratzer, W.B. (1991). Properties of the spectrin-like structural element of smooth-muscle α-actinin. Cell Motil. Cytoskeleton *20*, 242–248.

Kohn, W.D., Kay, C.M., and Hodges, R.S. (1998). Orientation, positional, additivity, and oligomerization-state effects of interhelical ion pairs in α-helical coiled-coils. J. Mol. Biol. *283*, 993–1012.

Kraulis, P.J. (1991). Molscript: a program to produce both detailed and schematic plots of protein structures. J. Appl. Crystallogr. *24*, 946–950.

Kuroda, M., Kohira, Y., and Sasaki, M. (1994). Conformational change of skeletal muscle α-actinin induced by salt. Biochim. Biophys. Acta. *1205*, 97–104.

Landon, F., Gache, Y., Touitou, H., and Olomucki, A. (1985). Properties of two isoforms of human blood platelet α-actinin. Eur. J. Biochem. *153*, 231–237.

Laskowski, R.A., MacArthur, M.W., Moss, D.S., and Thornton, J.M. (1993). PROCHECK: a program to check the stereochemical quality of protein structures. J. Appl. Crystallogr. *26*, 283–291.

Lyu, P.C., Gans, P.J., and Kallenbach, N.R. (1992). Energetic contribution of solvent-exposed ion pairs to α-helix structure. J. Mol. Biol. *223*, 343–350.

McLachlan, A.D., and Stewart, M. (1975). Tropomyosin coiled-coil interactions: evidence for an unstaggered structure. J. Mol. Biol. *98*, 293–304.

Merritt, E.A., and Murphy, M.E.P. (1994). Raster3D Version 2.0: a program for photorealistic molecular graphics. Acta Crystallogr. D *50*, 869–873.

Mukai, H., Toshimori, M., Shibata, H., Takanaga, H., Kitagawa, M., Miyahara, M., Shimakawa, M., and Ono, Y. (1997). Interaction of PKN with α-actinin. J. Biol. Chem. *272*, 4740–4746.

Nicholls, A., Sharp, K.A., and Honig, B. (1991). Protein folding and association: insights from the interfacial and thermodynamic properties of hydrocarbons. Proteins *11*, 281–296.

Ohtsuka, H., Yajami, H., Maruyama, K., and Kimura, S. (1997). The N-terminal Z repeat 5 of connectin/titin binds to the C-terminal region of α-actinin. Biochem. Biophys. Res. Commun. *235*, 1–3.

Otey, C.A., Pavalko, F.M., and Burridge, K. (1990). An interaction between α-actinin and the β1 integrin subunit in vitro. J. Cell Biol. *111*, 721–729.

Otwinowski, Z., and Minor, W. (1997). Processing of X-ray diffraction data collected in oscillation mode. Methods Enzymol. *276*, 307–326.

Pannu, N.S., and Read, R.J. (1996). Improved structure refinement through maximum likelihood. Acta Crystallogr. A *52*, 659–668.

Parks, T.D., Leuther, K.K., Howard, E.D., Johnston, S.A., and Dougherty, W.G. (1994). Release of proteins and peptides from fusion proteins using a recombinant plant virus proteinase. Anal. Biochem. *216*, 413–417.

Pascual, J., Castresana, J., and Saraste, M. (1997a). Evolution of the spectrin repeat. Bioessays *19*, 811–817.

Pascual, J., Pfuhl, M., Walther, D., Saraste, M., and Nilges, M. (1997b). Solution structure of the spectrin repeat: a left-handed antiparallel triple-helical coiled-coil. J. Mol. Biol. *273*, 740–751.

Pavalko, F.M., Walker, D.M., Graham, L., Goheen, M., Doerschuk, C.M., and Kansas, G.S. (1995). The cytoplasmic domain of L-selectin interacts with cytoskeletal proteins via α-actinin: receptor positioning in microvilli does not require interaction with α-actinin. J. Cell Biol. *129*, 1155–1164.

Read, R.J. (1986). Improved Fourier coefficients for maps using phases from partial structures with errors. Acta Crystallogr. A *42*, 140–149.

Rief, M., Pascual, J., Saraste, M., and Gaub, H.E. (1999). Single molecule force spectroscopy of spectrin repeats: low unfolding forces in helix bundles. J. Mol. Biol. *286*, 553–561.

Šali, A., and Blundell, T.L. (1993). Comparative protein modelling by satisfaction of spatial restraints. J. Mol. Biol. *234*, 779–815.

Speicher, D.W., and Marchesi, V.T. (1984). Erythrocyte spectrin is comprised of many homologous triple helical segments. Nature *311*, 177–180.

Speicher, D.W., Weglarz, L., and DeSilva, T.M. (1992). Properties of human red cell spectrin heterodimer (side-to-side) assembly and identification of an essential nucleation site. J. Biol. Chem. *267*, 14775–14782.

Taylor, K.A., and Taylor, D.W. (1993). Projection image of smooth muscle α-actinin from two-dimensional crystals formed on positively charged lipid layers. J. Mol. Biol. *230*, 196–205.

Trave, G., Pastore, A., Hyvonen, M., and Saraste, M. (1995). The C-terminal domain of α-spectrin is structurally related to calmodulin. Eur. J. Biochem. *227*, 35–42.

Viel, A., and Branton, D. (1994). Interchain binding at the tail end of the Drosophila spectrin molecule. Proc. Natl. Acad. Sci. USA *91*, 10839–10843.

Wachsstock, D.H., Wilkins, J.A., and Lin, S. (1987). Specific interaction of vinculin with α-actinin. Biochem. Biophys. Res. Commun. *146*, 554–560.

Winder, S.J., Gibson, T.J., and Kendrick-Jones, J. (1995). Dystropin and utrophin: the missing links! FEBS Lett. *369*, 27–33.

Winkler, J., Lünsdorf, H., and Jockusch, B.M. (1997). Flexibility and fine structure of smooth-muscle α-actinin. Eur. J. Biochem. *248*, 193–199.

Wyszynski, M., Lin, J., Rao, A., Nigh, E., Beggs, A.H., Craig, A.M., and Sheng, M. (1997). Competitive binding of α-actinin and calmodulin to the NMDA receptor. Nature *385*, 439–442.

Xia, H., Winokur, S.T., Kuo, W.L., Altherr, M.R., and Bredt, D.S. (1997). Actinin-associated LIM protein: identification of a domain interaction between PDZ and spectrin-like repeat motifs. J. Cell Biol. *139*, 507–515.

Yan, Y., Winograd, E., Viel, A., Cronin, T., Harrison, S.C., and Barnton, D. (1993). Crystal structure of the repetitive segments of spectrin. Science *262*, 2027–2030.

Young, P., Ferguson, C., Banuelos, S., and Gautel, M. (1998). Molecular structure of the sarcomeric Z-disk: two types of titin interactions lead to an asymmetrical sorting of α-actinin. EMBO J. *17*, 1614–1624.

Protein Data Bank ID Code

The R2R3 structure reported in this paper has been deposited in the Protein Data Bank under ID code 1QUU.